Journal of
Synchrotron
Radiation

ISSN 1600-5775

Received 11 December 2013
Accepted 18 February 2014

Fast continuous energy scan with dynamic coupling of the monochromator and undulator at the DEIMOS beamline

L. Joly,[a]* E. Otero,[b] F. Choueikani,[b] F. Marteau,[b] L. Chapuis[b] and P. Ohresser[b]

[a]Institut de Physique et de Chimie des Materiaux de Strasbourg, Université de Strasbourg, UMR 7504, 23 Rue du Loess, BP 43, 67034 Strasbourg Cedex 2, France, and [b]Synchrotron SOLEIL, L'Orme des Merisiers, Saint-Aubin, BP 48, 91192 Gif-sur-Yvette, France.
*E-mail: loic.joly@ipcms.unistra.fr

In order to improve the efficiency of X-ray absorption data recording, a fast scan method, the *Turboscan*, has been developed on the DEIMOS beamline at Synchrotron SOLEIL, consisting of a software-synchronized continuous motion of the monochromator and undulator motors. This process suppresses the time loss when waiting for the motors to reach their target positions, as well as software dead-time, while preserving excellent beam characteristics.

Keywords: XMCD; continuous energy scan; undulator scan.

1. Introduction

DEIMOS (dichroism experimental installation for magneto-optical spectroscopy) is a soft X-ray beamline at the French synchrotron SOLEIL, dedicated to the study of the electronic and magnetic properties of matter using polarized light. It is optimized for high stability in energy and beam positioning, and for best reproducibility of the measurements. The beamline is designed for X-ray absorption spectroscopy (XAS) and X-ray magnetic dichroism, which are both element-sensitive and offer a very high sensitivity, allowing very small amounts of material to be measured (Gambardella *et al.*, 2002, 2004; Ohresser *et al.*, 2005), either at surfaces or diluted in bulk. Furthermore, X-ray magnetic circular dichroism (XMCD) can provide access to the magnetic orbital and spin moment *via* the so-called sum rules (Thole *et al.*, 1992; Carra *et al.*, 1993; Chen *et al.*, 1995).

XAS is a measure of the X-ray absorption as a function of the photon energy. The absorption is measured either *via* total fluorescence yield (TFY) or total electron yield (TEY), as well as direct absorption assuming the sample is transparent to the X-rays [$\sigma x = \ln(I_0/I)$, where σ is the linear absorption coefficient, x is the sample thickness, I_0 is the incident X-ray intensity and I is the transmitted X-ray intensity]. A dichroic spectrum is the difference between at least two absorption spectra measured with different light polarizations and/or different magnetic/electronic states as a function of the photon energy E. The most commonly known are:

(i) XMCD, where circular polarized light is used on samples showing non-zero net magnetization. The magnetic state of the sample is usually flipped with an external magnetic field.

(ii) X-ray linear dichroism (XLD), where linear polarized light is used on a sample having an anisotropic charge distribution. In some cases this charge anisotropy can be related to magnetic properties, and XLD can then be used to probe magnetic properties as well; this is called X-ray magnetic linear dichroism

Since dichroic spectra are obtained by the difference of absorption spectra, the stability of the photon beam (energy, shape, flux, *etc.*) and all other experimental conditions (sample, magnetic field, temperature, *etc.*) are critical issues, particularly if the measured dichroic signal is very small. To obtain the best results it is therefore mandatory to reduce as much as possible the impact of experimental instabilities.

Although SOLEIL and DEIMOS were designed to reach a very good photon beam stability, there are always tiny unexpected experimental condition changes as a function of time. To minimize these it is necessary to collect the data as fast as possible.

The standard way to acquire an absorption spectrum is to perform a step-by-step scan: the sensor giving the absorption signal is recorded only after all energy position actuators (monochromator and undulator motors) have reached their targeted position (energy setpoint). The drawback of this method is the large scan duration caused by the dead-times induced by the trajectory and accuracy strategy of the motors after each small displacement. Typically, a 100 eV scan over the $L_{2,3}$ edges of a transition metal lasts 20 min in this mode, with approximately 90% of dead-time.

An alternative approach is to use a continuous scan where a single motor displacement is ordered while the readback of the motor positions and the physical signals of the sensors are synchronously recorded. This method allows a very fast acquisition and smoother data acquisition because there is only one single displacement. Such a scan strategy has been developed previously on several beamlines at different

synchrotron facilities (Rogalev *et al.*, 1998; Solé *et al.*, 1999; Pascarelli *et al.*, 1999; Krempaský *et al.*, 2010; Izquierdo *et al.*, 2012).

In this paper we will present the recent in-house development at the DEIMOS beamline concerning the so-called *Turboscan*, a continuous measurement of physical signals during a continous motion of the monochromator and undulator motors. We will show that this scan mode is very efficient in preserving the beam characteristics.

2. Technical description

At the DEIMOS beamline (Ohresser *et al.*, 2013, 2014), the photons can be provided by two different undulators: the HU-52 APPLE II helical undulator providing variable polarization over the full energy range of 350–2500 eV and the EMPHU-65 undulator (currently under commissioning) capable of switching the polarization at a frequency of 5 Hz. The other critical element is the plane-grating monochromator (PGM) which selects the photon beam energy with a useful energy resolution power up to 10000 in the energy range 350–1500 eV, while for the higher energy range (up to 2500 eV) an alternate multilayer grating is used with a useful energy resolution power between 5000 and 10000. The main endstation is a cryomagnet able to reach 7 T along the X-ray axis or 2 T perpendicular to the X-ray axis with a sample temperature from 1.5 K to 370 K.

The full beamline is controlled *via* the Tango framework (Tango, 2013) grouping together all components called 'Tango devices'. Each Tango device gives easy access to the configuration and the control of the considered element.

The measured physical signals (sensors) are the sample TEY and TFY, the transmission of the sample, and the TEY current measured from a gold mesh before the sample (I_0) to normalize the three previous signals. All signals are measured with a NOVELEC MCCE-2 high-sensitivity low-current electrometer, converting a low current to an optical signal with the frequency proportional to the measured current (10 MHz converter). The frequency signals are then simultaneously measured by a counting card (reference PXI 6602 from National Instruments; http://www.ni.com/), able to synchronously record up to eight 32-bit channels.

The DEIMOS beamline is controlled *via* a Python software solution, which is based on the use of the PyTango library, allowing the interface between Python and Tango. The system is able to control the full beamline *via* the Tango devices, and the use of Python in the interactive mode (command line) allows fast writing of very long macros, hence the automation of large sequences of commands.

3. The *Turboscan* process

A continuous scan in energy implies synchronization of the following motors:

(i) monochromator motors [working in the Petersen mode (Petersen *et al.*, 1995)], controlling the rotations of the grating and the mirror [with α and β the incoming and outgoing incidence angles of the grating (with respect to the grating normal) and θ the grazing-incidence angle of the mirror (with respect to the mirror surface) (Polack *et al.*, 2007)];

(ii) HU-52 undulator, the gap (G) corresponding to the distance between the jaws (note: no phase displacement).

The energy of the photons produced by an undulator spreads within a rather narrow peak around the target energy (see, for example, Fig. 4*c*). The energy of the photons reaching the sample is then refined by the monochromator which is given the role of 'master' while the undulator is like a 'slave' (Krempaský *et al.*, 2010), and must follow the energy of the monochromator in order to give the maximum of the photon flux.

The relations between the photon energy (*via* the wavelength λ) and the angles α and β are given by

$$Nk\lambda = -2\sin\left(\frac{\alpha+\beta}{2}\right)\cos\left(\frac{\alpha-\beta}{2}\right), \quad (1)$$

$$c_{\rm ff} = \frac{1}{c} = \frac{\cos\beta}{\cos\alpha}, \quad (2)$$

where N is the grating density, k is the diffraction order, $c_{\rm ff}$ is the fixed focus constant (Petersen criteria) and c is the inverse of $c_{\rm ff}$.

The relation between the gap (G) and the energy of the undulator can be approximated by the following relation,

$$E = \frac{a_0}{a_1\exp(a_2 G) + 1}, \quad (3)$$

where a_0, a_1 and a_2 are parameters experimentally determined for each polarization.

The relations between the photon energy and the monochromator angles α and θ are non-linear [equations (1) and (2)], as well as the relation between the photon energy and the undulator gap G [equation (3)]. Consequently, to obtain a perfect synchronization a rigorous approach would require sophisticated multi-axis motion control with non-linear motion trajectories. This is the hardware approach chosen by the IT group at SOLEIL but, because of its complexity, is still under development (Izquierdo *et al.*, 2012).

Therefore, in an anticipated approach we have developed a software-based solution using only the available linear motion trajectories for the monochromator angles α and θ, and for the undulator gap G. Using Tango tools, the following sequence is programmed (see Fig. 1): the monochromator and the undulator are both set to the starting energy (E_1). Taking c as a constant, equations (1) and (2) provide the couples (α, θ) for the energy E_1 and the final energy E_2. Then the linear motion trajectories as a function of time are determined for the motors controlling α and θ according to the input of the users (energy range, integration time and total time). Note here than a linear motion of the α and θ angles leads to a non-constant energy scan speed (variable energy increment as a function of time).

According to equation (3), the velocity of the undulator gap is not constant over the scan energy range. As a first approximation the gap velocity is set to the theoretical velo-

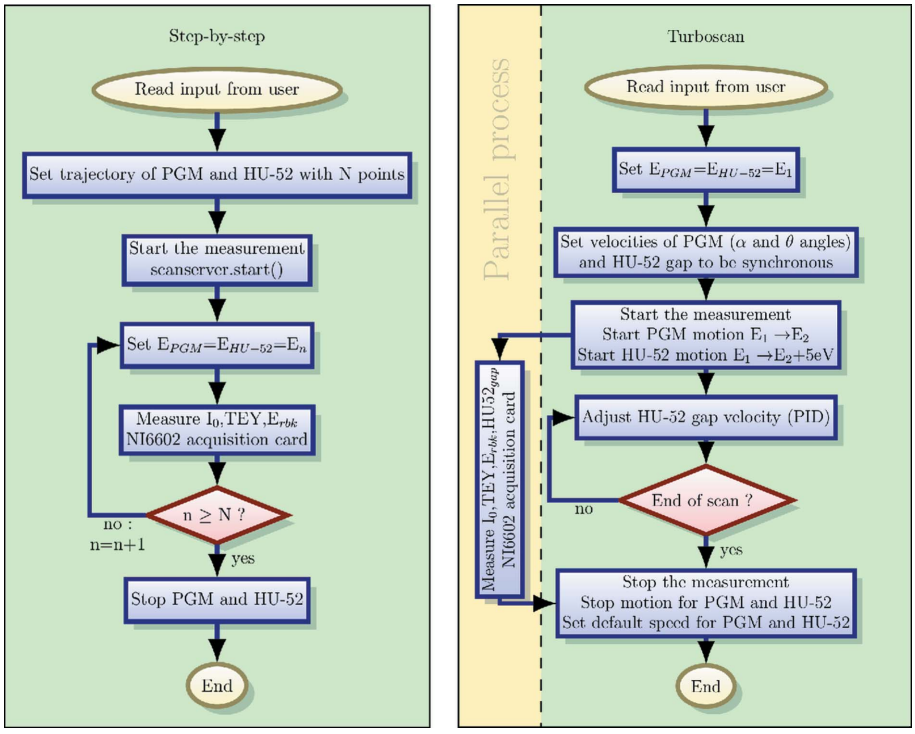

Figure 1
Sequence diagrams used for a step-by-step scan (left) and a *Turboscan* (right).

city at the middle of the scan, an approximation which is reasonable if the energy range is not too large (*i.e.* less than 100 eV). To make the synchronous motion of the undulator and the monochromator possible, the minimum gap velocity of the HU-52 APPLE II undulator has been decreased by a factor of 100 to be compatible with the typical acquisition time. The minimum velocity is now 0.2 µm s^{-1} and the maximum is 2 mm s^{-1}. We want to emphasize the fact that keeping the phase constant while performing an energy scan (changing the gap) can result in a drop of the circular polarization rate. Nevertheless, the calculations, confirmed by measurements, have demonstrated that over a 100 eV energy scan the drop of polarization is less than 0.5% (1%) for the first (second) harmonic. Only in the case of the third harmonic can we observe a drop of a few percent of the polarization rate. Owing to this latter result we have already foreseen some future development to implement a phase motion during a scan.

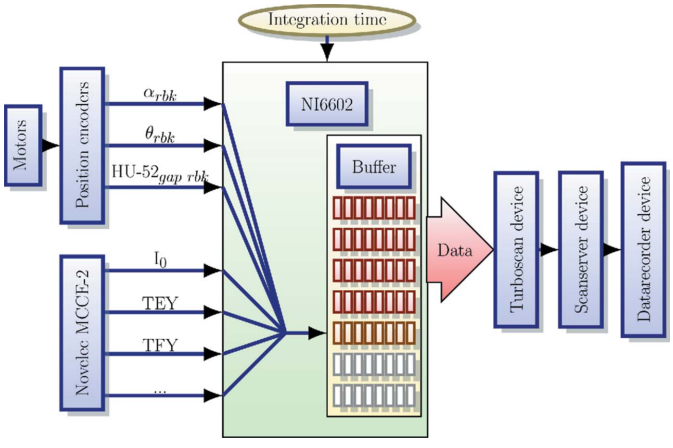

Figure 2
Data acquisition process diagram during a *Turboscan*.

The three trajectories (the two monochromator rotations and the undulator gap) are launched in a continuous motion using the 'scanserver' (a Tango device dedicated to controlling the trajectory and to collecting data). The data acquisition by the NI6602 card is placed in a parallel process (Fig. 1, right) in contrast to the step-by-step scan (Fig. 1, left). From the three corresponding motors, the encoders outputs (α_{rbk}, θ_{rbk} and HU-52_{rbk}) are connected to the NI6602 card to synchronize the positions of both the PGM and the undulator gap with the physical signals of the sensors (I_0, TEY, TFY, ...). The collected data are then stored in a buffer and read by the *Turboscan* device (in-house Tango device written in Python) to dynamically reconstruct the energy from the encoder positions allowing live visualization during the acquisition. The *Turboscan* device transfers the reconstructed data to the scanserver device, and then to the datarecorder device (see Fig. 2). The latter physically records the data and all the desired values into a Nexus file located in the SOLEIL secured storage place (SOLEIL, 2013). When the scan is finished (the monochromator energy reaches E_2), the data acquisition and all motions are stopped, and the monochromator and undulator motors are set back to their default velocity values.

4. Results

In the ideal case when the monochromator is working in the Petersen mode, c should be constant whatever the energy. Since the angles α and θ are moving with a constant speed, there are small variations of c around the nominal value. In order to characterize the good behaviour of the monochromator during a *Turboscan*, we calculated the c value of the monochromator as a function of the energy for different energy ranges. A deviation from the nominal c value induces essentially a change of the resolution by the same factor. Fig. 3 shows the relative difference of the actual c value with respect to the nominal value of $c = 0.2$ as a function of the energy for an average energy velocity of 0.5 eV s^{-1}. For a 100 eV-wide scan (typical energy range for our XAS measurements) and for an energy above 550 eV, we never observed a difference larger than 0.5% from the nominal c value over a full scan, demonstrating the good synchronization and behaviour of the process. For the scans with an energy below 550 eV the difference is still below 1.5%. The origin of the increase of the

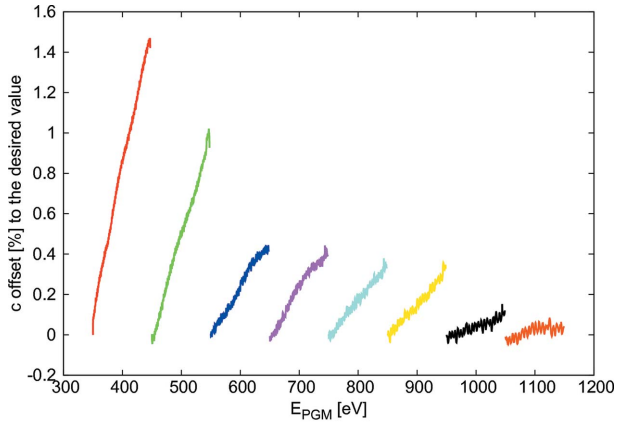

Figure 3
Relative difference between the real c value and the nominal setpoint (set to 0.2) for a 100 eV-wide *Turboscan* for various energies (average energy velocity 0.5 eV s^{-1}).

difference at low energy comes from the larger motion amplitude of the α and θ angles during the scan.

The other quality criterium is the energy shift (ideally zero) between the undulator energy and the monochromator energy which would produce a loss in photon flux. Fig. 4(*a*) (thick lines) shows this energy shift for several typical energy ranges (scan width 100 eV) for an average energy velocity of 0.5 eV s^{-1}. Due to the present step motor controller choice at SOLEIL, the gap of the undulator must follow a linear motion. However, since the energy of the photons produced by the undulator is not a linear function of the gap [equation (3)], the energy shift takes the shape of a parabola. This represents the main limitation of the approximation we were using in a first attempt: the velocity of the gap is only exact in the middle of the energy scan range. If an energy shift between the undulator and the monochromator occurs, a loss of flux is observed (Fig. 4*c*). Indeed, in the case of the HU-52 undulator the full width at half-maximum (FWHM) of an undulator peak is between approximately 15 and 50 eV (Fig. 4*c*); consequently in the worst case a loss in flux of 25% is observed (Fig. 4*b*, thick lines). Note that a loss of flux does not impact on the measurements themselves, since the physical signals are normalized to I_0. When the energy reaches 1000 eV or above, the offset between monochromator and undulator energy increases non-linearly with increasing energy.

5. Toward dynamical coupling with a PID loop

For large energy range scans, the non-linearity is critical. In this case, for the two extrema of the energy scan, the optimum gap velocity of the undulator is very different (*e.g.* 0.008 mm s^{-1} at 700 eV to 0.016 mm s^{-1} at 1150 eV at 0.5 eV s^{-1}); then the velocity has to be changed during the scan to keep the energy shift as low as possible. To overcome the limitations of the fixed gap velocity we changed and improved the process of the *Turboscan* by using a proportional-integrate-derivative feedback loop (PID) to dynamically couple the undulator energy to the measured energy of

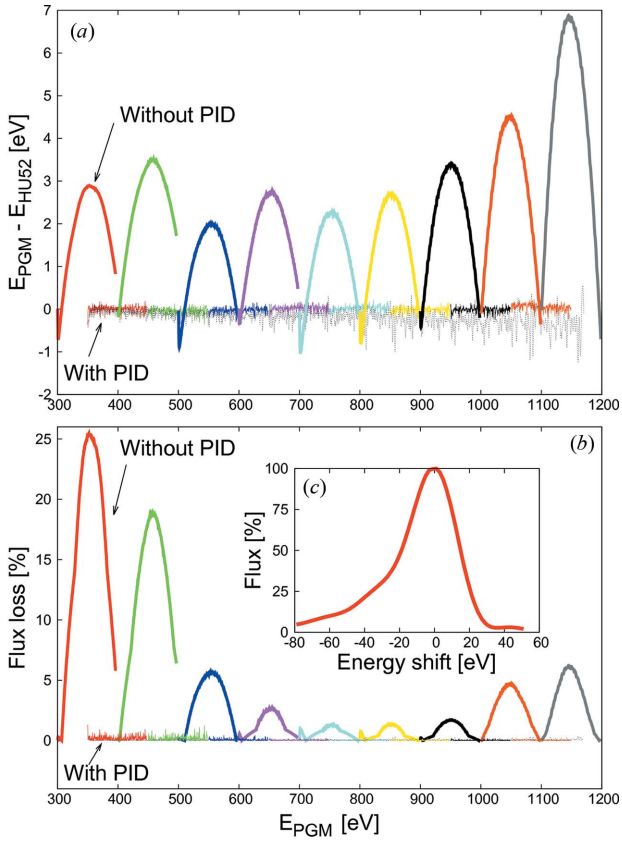

Figure 4
(*a*) Energy shift between the undulator and monochromator energies for some *Turboscans* without PID controller (thick lines) and with PID controller (thin lines and short-dashed line) (energy velocity about 0.5 eV s^{-1}). (*b*) Flux loss for the corresponding scans without (thick lines) and with (thin lines and short-dashed line) PID. (*c*) Undulator flux peak profile when the energy of the undulator is tuned at 850 eV as a function of the energy shift between the undulator and the monochromator.

the monochromator during the displacement. This dynamical coupling is mandatory if the user wants to improve the flux stability. With this process, we obtain a real master–slave dynamical coupling between the energy of the monochromator and the energy of the undulator. With respect to the previous process, during the motion of the monochromator angles, the energy of the undulator is compared with that of the monochromator in a parallel loop every 250 ms. The velocity of the undulator is then adjusted *via* a PID algorithm loop to minimize the energy offset to the monochromator.

The initial gap velocity of the undulator is now set to match the energy variation of the monochromator at the beginning of the scan. The change of the velocity of the gap during a displacement has been made possible by the SOLEIL Insertion Device group.

The result of the energy shift for a large 800 eV energy range and an average energy velocity of 0.85 eV s^{-1} is represented in Fig. 4(*a*) by the short-dashed line. During most of the scan, the energy shift stays below 1 eV, far better than the previous process. Fig. 4(*b*) (short-dashed lines) shows that during this scan the flux loss is always below 0.3%. The PID

algorithm therefore allows the flux stability to be optimized, but there is a large variation of c (about 7%) hindering a full quantitative interpretation of wide scans. In the case of the more typical 100 eV scans with an average energy velocity of 0.5 eV s^{-1} (Fig. 4*a*, thin lines), the energy shift is strongly reduced to less than ± 100 meV which is very good compared with the FWHM of the undulator peaks and avoids any loss of flux (which is always below 0.5%; Fig. 4*b*, thin lines).

6. Conclusions

In conclusion, we have developed an in-house method called *Turboscan* to reduce the data acquisition time and to improve the quality of the measurements at the DEIMOS beamline. Compared with a step-by-step scan, the *Turboscan* allows a gain of about ten in time with similar statistics and resolution in energy. We checked some quality criteria to validate the method and after weeks of commissioning the *Turboscan* has now been intensively and satisfactory used on the beamline since July 2012. The development of a fast data acquisition mode while keeping high-quality spectra was a priority of the DEIMOS beamline in order to improve the beamline efficiency. The high-speed data acquisition (typical time about 2–4 min for one X-ray absorption spectra) now allows users to study new time-dependent effects (see, for example, Davesne *et al.*, 2013) which was impossible with a step-by-step scan (typical time of about 25 min). Last but not least, a lot of users want to study highly X-ray-sensitive samples (such as molecular magnet in monolayer assemblies); the damage caused by the photon beam to that kind of sample can be reduced thanks to shorter time exposition.

The authors gratefully acknowledge the SOLEIL Insertion Devices group for the work that has made possible the present development.

References

Carra, P., Thole, B. T., Altarelli, M. & Wang, X. (1993). *Phys. Rev. Lett.* **70**, 694–697.

Chen, C. T., Idzerda, Y. U., Lin, H., Smith, N. V., Meigs, G., Chaban, E., Ho, G. H., Pellegrin, E. & Sette, F. (1995). *Phys. Rev. Lett.* **75**, 152–155.

Davesne, V., Gruber, M., Miyamachi, T., Da Costa, V., Boukari, S., Scheurer, F., Joly, L., Ohresser, P., Otero, E., Choueikani, F., Gaspar, A. B., Real, J. A., Wulfhekel, W., Bowen, M. & Beaurepaire, E. (2013). *J. Chem. Phys.* **139**, 074708.

Gambardella, P., Dallmeyer, A., Maiti, K., Malagoli, M. C., Eberhardt, W., Kern, K. & Carbone, C. (2002). *Nature (London)*, **416**, 301–304.

Gambardella, P., Dallmeyer, A., Maiti, K., Malagoli, M. C., Rusponi, S., Ohresser, P., Eberhardt, W., Carbone, C. & Kern, K. (2004). *Phys. Rev. Lett.* **93**, 077203.

Izquierdo, M., Hardion, V., Renaud, G., Chapuis, L., Millet, R., Langlois, F., Marteau, F. & Chauvet, C. (2012). *J. Synchrotron Rad.* **19**, 619–626.

Krempaský, J., Fleschsig, U., Korhonen, T., Zimoch, D., Quitmann, Ch. & Nolting, F. (2010). *AIP Conf. Proc.* **1234**, 705–708.

Ohresser, P., Bulou, H., Dhesi, S. S., Boeglin, C., Lazarovits, B., Gaudry, E., Chado, I., Faerber, J. & Scheurer, F. (2005). *Phys. Rev. Lett.* **95**, 195901.

Ohresser, P., Otero, E., Choueikani, F., Chen, K., Stanescu, S., Deschamps, F., Moreno, T., Polack, F., Lagarde, B., Daguerre, J. P., Marteau, F., Scheurer, F., Joly, L., Kappler, J. P., Muller, B., Buneau, O. & Sainctavit, Ph. (2014). *Rev. Sci. Instrum.* **85**, 013106.

Ohresser, P., Otero, E., Choueikani, F., Stanescu, S., Deschamps, F., Ibis, L., Moreno, T., Polack, F., Lagarde, B., Marteau, F., Scheurer, F., Joly, L., Kappler, J.-P., Muller, B. & Sainctavit, Ph. (2013). *J. Phys. Conf. Ser.* **425**, 212007.

Pascarelli, S., Neisius, T. & De Panfilis, S. (1999). *J. Synchrotron Rad.* **6**, 1044–1050.

Petersen, H., Jung, C., Hellwig, C., Peatman, W. B. & Gudat, W. (1995). *Rev. Sci. Instrum.* **66**, 1–14.

Polack, F., Lagarde, P. & Idir, M. (2007). *AIP Conf. Proc.* **879**, 655–658.

Rogalev, A., Gotte, V., Goulon, J., Gauthier, C., Chavanne, J. & Elleaume, P. (1998). *J. Synchrotron Rad.* **5**, 989–991.

Solé, V. A., Gauthier, C., Goulon, J. & Natali, F. (1999). *J. Synchrotron Rad.* **6**, 174–175.

SOLEIL (2013). *Storage of the Experimental Data*, http://www.synchrotron-soleil.Fr/portal/page/portal/Instrumentation/InformatiqueElectronique/StockageDonnees.

Tango (2013). *The TANGO framework*, http://www.tango-controls.org/.

Thole, B. T., Carra, P., Sette, F. & van der Laan, G. (1992). *Phys. Rev. Lett.* **68**, 1943–1946.